Submesoscale streamers exchange water on the north wall of the Gulf Stream

Jody M. Klymak[1], R. Kipp Shearman[2], Jonathan Gula[3], Craig M. Lee[4], Eric A. D'Asaro[4], Leif N. Thomas[5], Ramsey R. Harcourt[4], Andrey Y. Shcherbina[4], Miles A. Sundermeyer[6], Jeroen Molemaker[7], and James C. McWilliams[7]

[1] School of Earth and Ocean Sciences, University of Victoria, Victoria, British Columbia, Canada, [2] College of Earth, Ocean, and Atmospheric Sciences, Oregon State University, Corvallis, Oregon, USA, [3] Laboratoire d'Océanographie Physique et Spatiale, Université de Bretagne Occidentale, Brest, France, [4] Applied Physics Laboratory, University of Washington, Seattle, Washington, USA, [5] School of Earth Sciences, Stanford University, Stanford, California, USA, [6] School for Marine Science and Technology, University of Massachusetts Dartmouth, Dartmouth, Massachusetts, USA, [7] Department of Atmospheric and Oceanic Sciences, University of California, Los Angeles, California, USA

Abstract The Gulf Stream is a major conduit of warm surface water from the tropics to the subpolar North Atlantic. Here we observe and simulate a submesoscale (<20 km) mechanism by which the Gulf Stream exchanges water with subpolar water to the north. Along isopycnals, the front has a sharp compensated temperature-salinity contrast, with distinct mixed water between the two water masses 2 and 4 km wide. This mixed water does not increase downstream despite substantial energy available for mixing. A series of streamers detrain this water at the crest of meanders. Subpolar water replaces the mixed water and resharpens the front. The water mass exchange accounts for a northward flux of salt of $0.5–2.5$ psu m^2 s^{-1}, (large-scale diffusivity O (100 m^2 s^{-1})). This is similar to bulk-scale flux estimates of 1.2 psu m^2 s^{-1} and supplies fresher water to the Gulf Stream required for the production of 18° subtropical mode water.

1. Introduction

The Gulf Stream (GS) is the western boundary current of the North Atlantic subtropical wind-driven circulation. It separates from Cape Hatteras where it flows eastward into the North Atlantic. As it flows, it loses heat to the atmosphere and by mixing with the cold water in the subpolar gyre to the north. It also becomes fresher, an observation that can only be explained by entrainment of fresh water from the north [*Joyce et al.*, 2013]. As it entrains water, the GS increases its eastward transport at a rate of approximately $40–80$ m^2 s^{-1} (or $4–8$ Sv /100 km [*Johns et al.*, 1995]).

The GS has a sharp density front that outcrops at the surface. It also has a sharp temperature and salinity front, as has been demonstrated at the surface from shipboard surveys [*Ford et al.*, 1952] and satellite images [*Churchill et al.*, 1989]. The sharpness of the front beneath the surface has been less clear and requires high-resolution lateral sampling to resolve. The front has a sharp potential vorticity gradient [*Rajamony et al.*, 2001], and such gradients act as a barrier to lateral mixing [*Marshall et al.*, 2006; *Naveira Garabato et al.*, 2011]. Despite this barrier, property budgets indicate that there is significant exchange across the north wall [*Joyce et al.*, 2013] and that entrainment of fresh water is necessary to create the dynamically important 18° water that fills much of the upper Sargasso Sea.

The mechanisms controlling this lateral mixing have not been identified. There are large eddies that periodically pinch off the GS and carry warm water to the north. However, some of these are reentrained into the GS and do not result in a net exchange. Instead, tracer budgets across the front appear to be dominated by small, submesoscale processes [*Bower et al.*, 1985]. To date the best direct evidence for cross-front exchange comes from the trajectories of density-following floats placed at the north wall [*Bower and Rossby*, 1989; *Bower and Lozier*, 1994]. These floats were observed to regularly detrain from the GS, such as that of 95 floats, 26 stayed in the GS, 7 were detrained in rings, and 62 were detrained by mechanisms other than rings [*Bower and Lozier*, 1994]. Kinematic theories have been examined to explain the detrainment of the floats [*Flierl et al.*, 1987; *Stern*, 1985; *Pratt et al.*, 1995], and the similarity to satellite images of streamers of warm water detraining
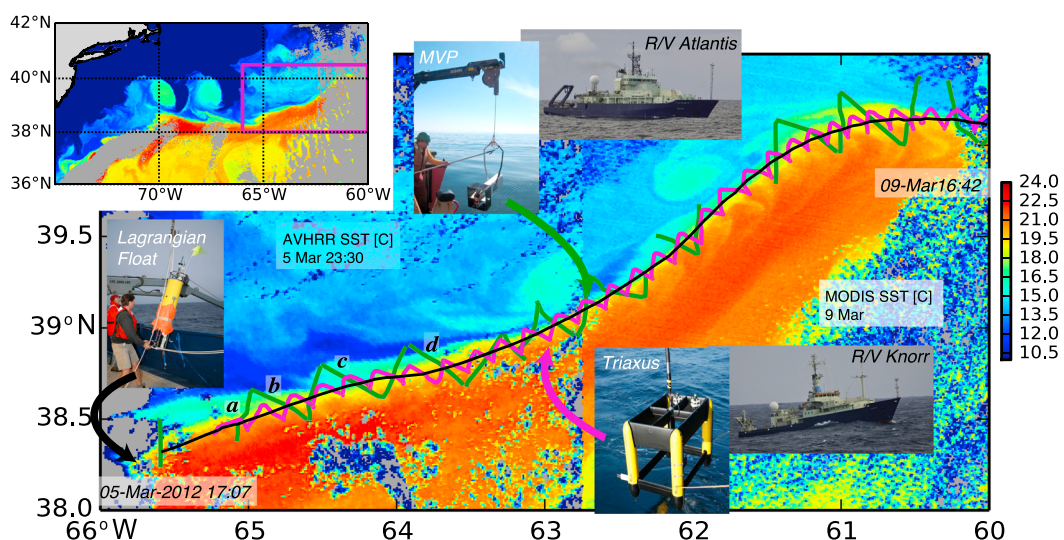
Figure 1. The experimental design. (inset) The experiment site on the north wall of the Gulf Stream, between 66 and 60°W, as shown in an AVHRR satellite image of sea surface temperature (SST). (main) Detailed SST image composed from two satellite images. The GS is warm and delineated by a sharp front. The small submesoscale structures north of the front are the focus of this paper. The satellite images are a composite from early in the observation period (AVHRR 6 March) and late (MODIS, 9 March). A Lagrangian float was deployed in the front (black curve), and the ship tracks bracketed the float's position (green: R/V *Atlantis*, magenta: R/V *Knorr*). R/V *Atlantis* cross sections labeled a–d are shown in Figures 2a–2d.

from the Gulf Stream has been noted. However, direct observations of the process as it occurs at depth have been lacking.

Here we point out that the density front is accompanied by a sharp (<5 km wide) and persistent temperature-salinity front along isopycnals. We also present indirect evidence that there is small-scale mixing (<0.5 km) on the northern cyclonic side of the GS and that the mixed water periodically peels off the GS in thin (5–10 km wide) "streamers." We describe our experiment and the observations that it yielded before briefly discussing the implications.

2. Methods

In March 2012 we made high-resolution measurements of the north wall of the GS from 66°W to 60°W (Figure 1), about 850 km east of where the GS separates from the North American continental slope. A Lagrangian float [*D'Asaro*, 2003] was placed in the Gulf Stream front based on a brief cross-stream survey and programmed to match the density of the surface mixed layer (upper 30 m). The float moved downstream at a mean speed of 1.4 m s^{-1}. The R/V *Knorr* tracked the float and deployed a Chelsea Instruments TriAxus that collected temperature, salinity, and pressure (CTD) on a 200 m deep sawtooth with approximately 1 km lateral spacing in a 10 km box-shaped pattern relative to the float (Figure 1, magenta). R/V *Atlantis* performed larger cross sections approximately 30 km across the front, trying to intercept the float on each front crossing. R/V *Atlantis* was deploying a Rolls Royce Marine Moving Vessel Profiler equipped with a CTD that profiled to 200 m approximately every 1 km. Both ships had a 300 kHz RDI acoustic Doppler current profiler (ADCP) collecting currents on 2 m vertical scale averaged every 5 min (approximately 1 km lateral scale), collected and processed using UHDAS and CODAS [*Firing et al.*, 2012; http://currents.soest.hawaii.edu]. Velocities are put into a float-following frame as a proxy for along front and across front, with u being defined as along the floats path and v as perpendicular to the path and to the north. Velocity data at 2 m vertical resolution reached about 130 m and were supplemented at deeper depths with data from 75 kHz RDI ADCPs, with 8 m vertical resolution.

Data were interpolated onto a cube delineated by depth surfaces by creating a two-dimensional interpolation onto a grid via Delauney triangulation at each depth; no extrapolation was performed. Data on the 26.25 kg m^{-3} isopycnal (chosen as a midpoint of the streamer density range) were assembled at each grid

point by finding the first occurrence of that isopycnal in depth. Potential vorticity is calculated from the three-dimensional grid as

$$q = -\frac{g}{\rho_0} \left(\nabla \times \mathbf{u} + \mathbf{f} \right) \cdot \nabla \rho, \tag{1}$$

where f is the Coriolis frequency and g the gravitational acceleration. The bracketed term is twice the angular velocity, including the planet's rotation, and the gradient of density represents the stretching or compression of the water column. In the GS, the potential vorticity is dominated by contributions from the vertical density gradient, $N^2 = \frac{1}{\rho_0} \frac{\partial \rho}{\partial z}$ and the cross-stream gradient of the along-stream velocity, which was used to approximate potential vorticity from two-dimensional sections:

$$q \approx N^2 \left(-\frac{\partial u}{\partial y} + f \right). \tag{2}$$

At select times during the float drifts, fluorescein dye releases (100 kg per release) were conducted at depths as close as possible to the float. Dye was pumped down a hose to a tow package deployed off the side of the ship, consisting of a CTD and a dye diffuser. Prior to injection, the dye was mixed with alcohol and ambient sea water to bring it to within 0.001 kg m^{-3} of the float's target density. Initial dimensions of the dye streak were ≈1 km along stream, ≈100 m cross stream (after wake adjustment), and ranging from 1 to 5 m in the vertical. The TriAxus system on the R/V *Knorr* tracked the fluorescein from its CTD package.

Numerical simulations of the GS were performed with the Regional Oceanic Modeling System (ROMS) [*Shchepetkin and McWilliams*, 2005]. The simulation has a horizontal resolution of 500 m and 50 vertical levels. The model domain spans 1000 km by 800 km and covers a region of the GS downstream from its separation from the U.S. continental slope. Boundary conditions are supplied by a sequence of two lower resolution simulations that span the entire GS region and the Atlantic basin, respectively. The simulation is forced by daily winds and diurnally modulated surface fluxes. The modeling approach is described in detail in *Gula et al.* [2015].

Neutrally buoyant Lagrangian (flow-following) particles were seeded into the model at a time t_0 and advected both backward and forward in time by the model velocity fields without additional dispersion from the model's mixing processes [*Gula et al.*, 2014]. A fourth-order Runge-Kutta method with a time step dt=1 s was used to compute particle advection. Velocity and tracer fields were interpolated at the positions of the particles using cubic spline interpolation in both the horizontal and vertical directions. We linearly interpolated hourly outputs in time from the simulation to get sufficiently frequent and temporally smooth velocity sampling for accurate parcel advection.

3. Observations

During these observations, the GS had a shallow meander crest at 65°W (Figure 1b) followed by a long concave region (63°W) and then another large crest (61°W). Satellite measurements show the sharp temperature changes across the front, superimposed with thin intermediate-temperature (15–18°C) streamers detraining to the north at approximately 65°W, 64°W, and at the crest of the large meander at 61°W. An older streamer that has rolled up can also be seen at 62°W. The ships passed through the three newer streamers providing a detailed observation of their underwater structure.

The front consists of density surfaces that slope up toward the north (Figures 2a–2d). The water along density surfaces is saltier (and warmer) in the GS, and fresher (and colder) to the north. The transition between the two water masses is remarkably abrupt, occurring over less than 5 km. This sharpness persists from the westernmost section during the cruise (71.5°W) to the easternmost (60.5°W). Some cross sections show lateral interleaving of salinity north of the front deeper than 70 m (Figure 2a) with approximately 5 km wide salinity anomalies ($S \approx 36.15$ psu, practical salinity unit). These anomalies move slower than the front (Figure 2e) and have high potential vorticity that is normally associated with the front (Figure 2i). The surface signature of the streamers (as seen in Figure 1b) can be also seen in these cross sections as saltier "surface" water (Figures 2a–2d), but the temperature-salinity (T/S) characteristics are not as distinct because of cooling by the atmosphere.

The temperature-salinity (T/S) relationship of this data shows the contrast between the GS and the subpolar water as two distinct modes (Figure 3, labeled "North" and "Gulf Stream"), except near the surface where the
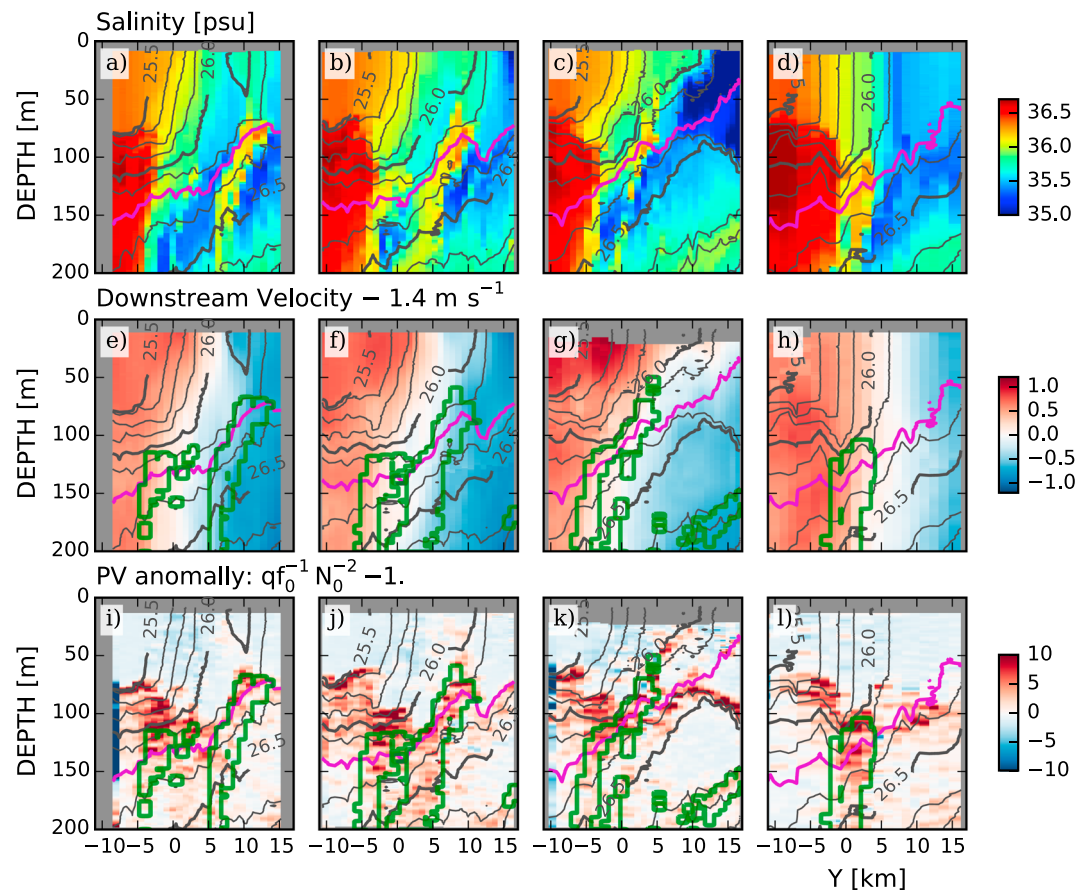
Figure 2. Cross sections of data collected across the Gulf Stream. Y is the cross-stream distance perpendicular to the path of the float, positive being northward. The four columns correspond to the four sections labeled a–d in Figure 1. Potential density is contoured in black and $\sigma_\theta = 26.25$ kg m^{-3} is magenta. (a) The farthest upstream section (65°W) and (d) the farthest downstream (63.75°W, Figure 1). (e–h) Downstream velocity calculated relative to the float's trajectory by removing the float's mean speed of $u_{float} = 1.4$ m s^{-1} for the observation period. Green contours are regions in temperature-salinity space labeled "streamers" in Figure 3. (i–l) Potential vorticity anomaly.
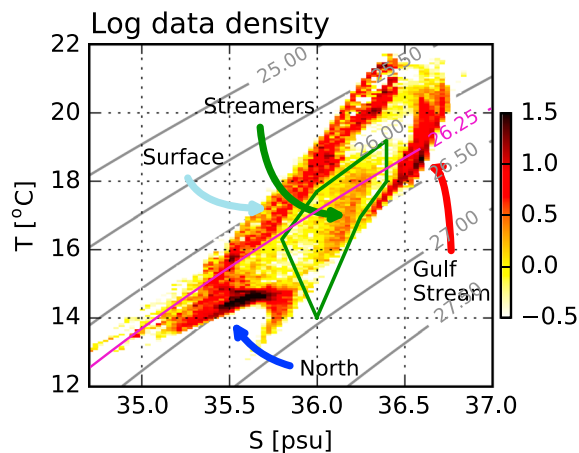
Figure 3. Logarithmically scaled histogram of 1 m by 1 km data points in temperature-salinity space (colors) of all the measurements in the occupation of the Gulf Stream. Between $\sigma_\theta = 26.1$ and $\sigma_\theta = 26.5$ kg m^{-3} there is a class of water distinct from the salty GS water and the fresh water to the north that we label "streamers" and delineate with a green box in T/S space. This water is contoured in green in Figures 2e–2l.
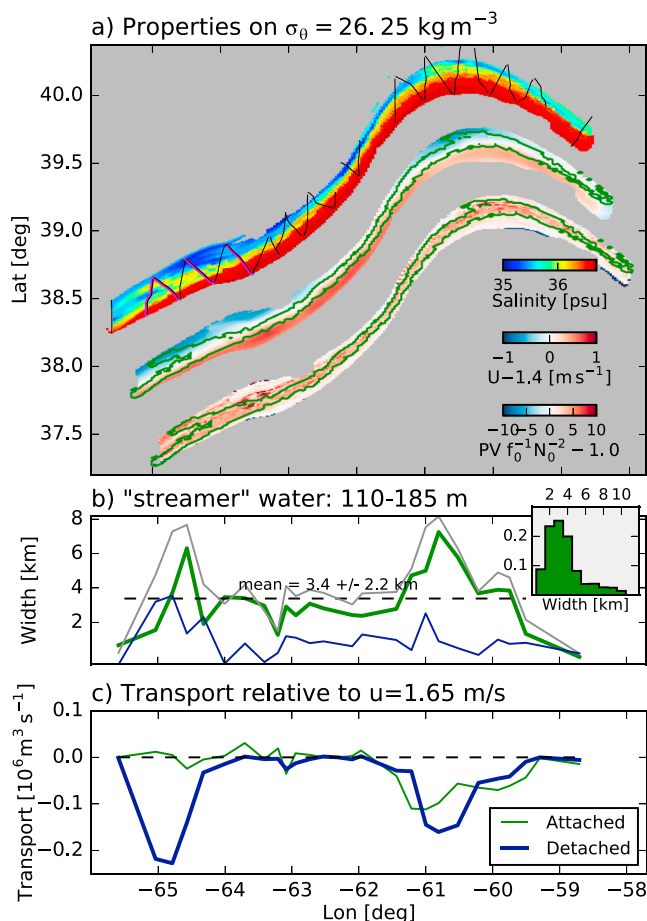
Figure 4. (a) Interpolation of salinity, velocity, and potential vorticity anomaly onto the $\sigma_\theta = 26.25$ kg m^{-3} isopycnal, plotted geographically (with a small exaggeration of scale in the north-south direction, and the latter two fields offset slightly to the south-east). The ship track for the *Atlantis* is plotted in black, and the four cross sections in Figure 2 are plotted in magenta. The streamer water is contoured in green. (b) Width of the streamer water averaged between 110 and 185 m, attached to the GS (green line), detached (blue line), and total (grey line); a water parcel is considered "attached" if there is no more than 1 km of water from the fresher water class to the north. (c) Transport of the streamer water relative to $u = 1.65$ m s^{-1} (blue), chosen to make the transport of the water attached to the GS (green) approximately zero.

water masses are strongly affected by the atmosphere. For the deeper water, there is a third distinct population between the two larger modes in T/S space representing water in the salinity anomalies that we have labeled as "streamers." The distinctness in the T/S space of the streamers indicates that after the GS and subpolar waters mixed, the partially mixed water continued to mix, coalescing it in T/S space so that it forms an almost separate water mass. Below, we further differentiate water in this T/S class as either "attached" to the GS or "detached."

Looking at the GS in plan view along the $\sigma_\theta = 26.25$ kg m^{-3} isopycnal (Figure 4a), we see that the mixed water that makes up the streamers is connected along the length of our observations, with a width that averages just less than 4 km (Figure 4b). The first detached streamer (64.5°W) is horizontally connected over 100 km and is about 5 km wide and at least 150 m deep. Where the streamer is the most detached (Figure 2a) the main front is the sharpest of the four cross sections. Downstream of this streamer, the mixed water thins before the eastern meander (60.5°W) where there is a second streamer. Farther downstream, the mixed water almost disappears by the last cross section (59°W).

We can estimate the rate of detrainment from the first streamer (64.5°W). It starts on the fast side of the front with water flowing approximately 0.1–0.25 m s^{-1} faster than the float (Figure 2h). Upstream, where it is detached (Figure 2e), it is flowing almost 0.2–0.5 m s^{-1} slower than the float. Integrating the transport relative
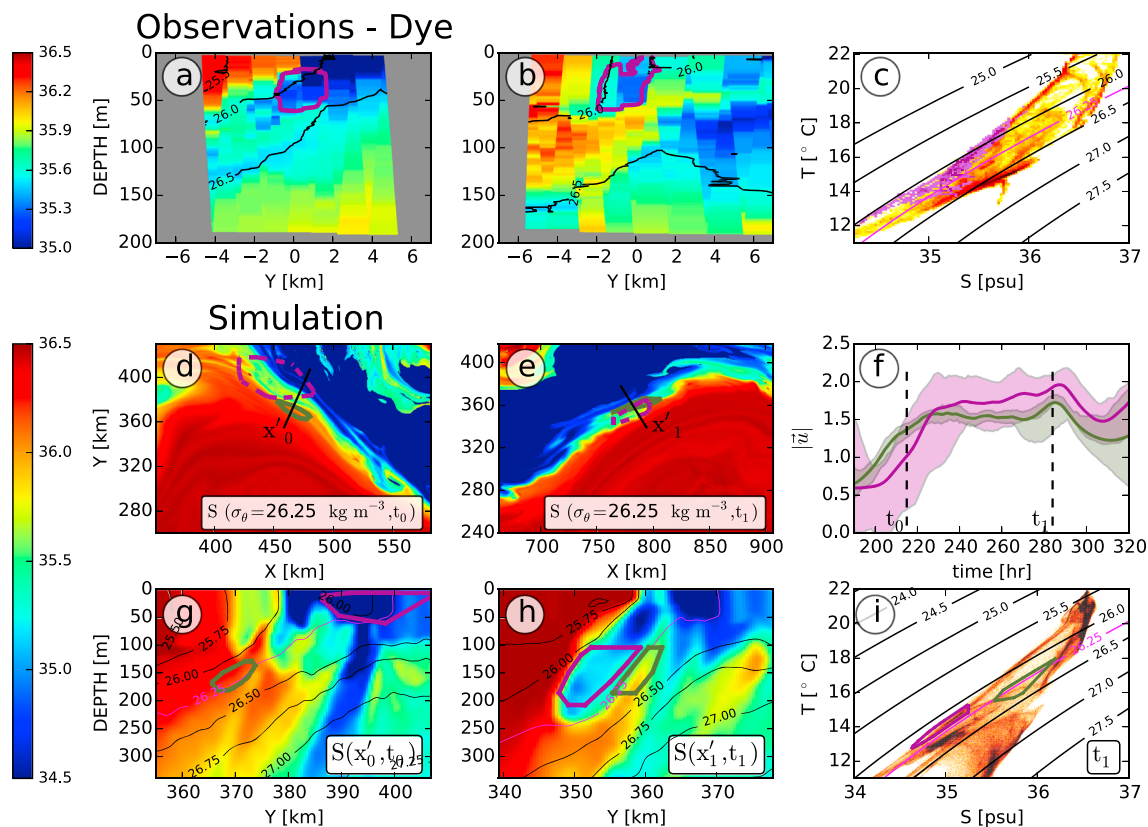
Figure 5. Evidence for entrainment of intrusions from a dye release and numerical simulation. (a) Salinity section from an occupation of the GS 14 March. The location of a dye is contoured in magenta. (b) Salinity section from downstream. A streamer has enfolded the dye in cold-fresh water between itself and the GS. (c) Temperature-salinity diagram for this occupation. The temperature-salinity for the dye is colored in dark magenta. (d) Salinity in the GS on the $\sigma_\theta = 26.25$ kg m^{-3} isopycnal from a high-resolution numerical simulation at t_0. X and Y are in model coordinates. The green contours delineate the location of particles seeded downstream in the streamer at time $t_1 = t_0 + 70$ h (see Figures 5e and 5h) and advected *backward* in time to t_0 showing where the streamer water originated. The dark magenta contour is the location of particles seeded in the fresh intrusion. The straight line shows the location of the salinity cross section in Figure 5g. (e) As in Figure 5d, except at $t_1 = t_0 + 70$ h; this is the time and locations where the two clouds of particles were seeded. (g and h) Salinity cross sections for times t_0 and t_1. The location of the particles is shown in green and dark magenta contours. The $\sigma_\theta = 26.25$ kg m^{-3} isopycnal is contoured in light magenta. These panels show that the origin of the streamer water was in the GS front and that the fresh-cold water (magenta contour) that enfolded against the front came from north of the front. (f) The speeds (minimum/maximum is shaded, and mean is the line) of the particle clouds in time, and shows that the intrusion water (magenta) accelerates relative to the streamer water (green). (i) The temperature-salinity of all the data at t_1, with the clouds of seeded particles indicated in T/S space. Note that the green streamer water occupies a mixed mode between the warm GS waters and the cold and fresh water to the north.

to the attached water just downstream, we see that the streamer detrains $0.2-0.25 \times 10^6$ m^3 s^{-1} of water (Figure 4c). This estimate is quite rough, given that the fully detached streamer was only sampled 3 times, the arbitrary division between "attached" and "detached" water, and the overall inhomogeneity of the water mass, but it serves as a rough estimate until better measurements can be made.

The streamers also appear to move up through the water column along isopycnals as water parcels are stretched vertically. While we can not unambiguously disentangle space-time aliasing in our subsurface in situ observations, we can see via satellite imagery that the surface expression of the streamers has synoptic elongated spatial structure. Meanwhile, model and dye results discussed below show that there is also vertical velocity and/or vertical mixing involved in streamer and intrusion formation. From our observations, the streamer has risen along isopycnals from 120 m deep (Figure 2d approximate depth where green streamer contour meets $\sigma_\theta = 26.25$ kg m^{-3} contour), to less than 70 m deep (Figure 2a) while tilting somewhat in the cross-stream direction as it has done so. The velocity anomaly is about 0.75 m s^{-1} (Figures 2e–2h) and spans ~100 km (Figure 4a), so we estimate that the streamer is approximately 1.5 days old. Assuming that the observed vertical shift is due entirely to vertical velocity within the streamer (and not entirely a lateral advective effect), this implies vertical velocities of order 33 m/d. This is comparable to rates inferred from

large-scale omega-equation calculations [*Thomas and Joyce*, 2010], though somewhat larger than similarly derived 10 m/d vertical velocity estimated from the numerical simulations described below.

Concurrently, there is a bolus of fresh water from the north that is enfolded between the streamers and the GS that we will call an "intrusion." This entrained water is part of the strong shear on the North Wall, so the amount of entrainment is harder to quantify than the detrainment from these observations.

A different survey (14 March) included a dye release in water that was subsequently entrained between the wall and a streamer (Figures 5a–5c). The dye was injected near the surface at the North Wall, centered at approximately 50 m depth on the 26.0 kg m^{-3} isopycnal in the fresh water. A subsequent pass 43 km downstream shows that the dye has been enfolded in a streamer (Figure 5b). In T/S space, this water is in the "surface" water class (Figure 5c). This particular streamer did become deeper, down to 100 m, and detrained farther from the front than shown here.

4. Simulations

High-resolution numerical simulations (dx ≈500 m) resolve these features and also confirm the entrainment of the fresh intrusion (Figures 5d–5i). Seeding the simulation with Lagrangian particles (see section 2) allows us to track the evolution of the streamers and the intrusion as the flow moves downstream. Before the streamer is formed, the water in the intrusion (magenta contours) is near the surface, and the streamer water (green contours) is well within the front (Figures 5d and 5g). Downstream (Figures 5e and 5h) the fresh water has been subducted to 150 m depth, and the streamer has been pushed north of the front. Both water masses accelerate with the GS (Figure 5f), but the fresh intrusion accelerates more, such that the intrusion is entrained and the streamer slows and is detrained. As in the observations, the streamer occupies an intermediate region in T-S space (Figure 5i, green contour), and originates in the high-vorticity region of the front. Meanwhile, the streamer is stretched vertically, with its shallowest extent rising from 100 m to 130 m over a period of 70 h, or approximately 10 m/d. The acceleration of the fresh intrusion relative to the streamer is an important finding of the model, as the fresh water now forms a new sharp T-S front with the warm salty GS, and the mixed streamer water is carried away from the front. The model further shows that the streamers are more prominent on the leading edges of meanders, also clearly seen in satellite images (Figure 1).

There are differences with the observations, however. The data show very distinct T-S signatures associated with the streamers, whereas the model streamer T/S "mode" is less isolated (Figure 5i). The two interleaving water masses are confined to a narrow isopycnal band in the model, with the intrusion being slightly lighter than the streamer, whereas in the observations the temperature-salinity front cuts across more isopycnals (compare Figure 2b to Figure 5h). There is also clear evidence of strong subduction of the intrusion in the model, reminiscent of intrathermocline eddies [*Thomas and Joyce*, 2010]. Overall, the model has similar dynamics but likely lacks subkilometer mixing processes that create the "streamer" water in exactly the way it is created in nature.

5. Discussion

The distinct T/S mode on the density-compensated front of the Gulf Stream is a new finding to our knowledge and enabled by our very high density of sampling. The implication of this water class is that mixing at the Gulf Stream front is relatively "complete" in that water trapped in an instability is trapped there for long enough that it is homogenized. Symmetric instability has been observed in the north wall and the Kuroshio, and this T/S mode may be indirect evidence for its role in lateral mixing [*D'Asaro et al.*, 2011; *Thomas et al.*, 2016].

The streamers that detrain from the north wall have been seen in satellites and inferred from floats [*Bower and Rossby*, 1989; *Flierl et al.*, 1987; *Lozier et al.*, 1997; *Song et al.*, 1995]; however, this is the first time they have been shown to penetrate so deep and to be composed primarily of the mixed class of water. The detrainment helps explain why the front at the north wall of the GS remains so sharp. That only the mixed water is carried away, and not high-salinity GS water (Figure 4a) is a mystery and implies a dynamical link that we have not seen explored in kinematic models of streamers [*Bower*, 1991; *Pratt et al.*, 1995; *Lozier et al.*, 1997]. This coincidence indicates to us a role for small-scale mixing in producing the destabilizing forces that cause this water to detrain from the north wall.

The streamers appear to be one of the processes that balance large-scale budgets of exchange across the GS [*Joyce et al.*, 2013; *Bower et al.*, 1985]. Such budgets suggest that this region of the GS loses salinity to the north

at a rate of 1.2 psu m^2 s^{-1} [*Joyce et al.*, 2013]. If each streamer transports $0.2-0.25 \times 10^6$ m^3 s^{-1} of water that is $0.8-1$ psu saltier than the water that is entrained, and streamers appear approximately every $100-300$ km, associated with meanders, then an estimate of their average transport is $0.5-2.5$ psu m^2 s^{-1}, bracketing the large-scale estimates. Working against a gradient of 1 psu/10 km over 200 m depth, the equivalent mesoscale lateral diffusivity is $25-125$ m^2 s^{-1}. These estimates are approximate and based on one observation of one streamer. Presumably, some streamers are stronger than others, and better statistics are desirable. Similarly, whether the streamers are the rate-limiting mechanism driving salt flux out of the GS, as opposed to the small-scale turbulence at the wall, is unknown.

Here we have observed a submesoscale lateral stirring process along the north wall of the GS. The T/S front remains persistently sharp, despite small-scale mixing evident from the T/S diagrams that is caused by a number of possible processes [*Thomas and Shakespeare*, 2015; *Whitt and Thomas*, 2013]. The mixed water mass does not accumulate, or it would weaken the sharpness of the front. Here we show that the streamers detrain mixed water and entrain cold and fresh water toward the north wall, resharpening the temperature-salinity front. Further analysis of the data and models will shed light on the exact mechanism triggering the ejection of water from the front via the streamers.

References

Bower, A., and T. Rossby (1989), Evidence of cross-frontal exchange processes in the Gulf Stream based on isopycnal RAFOS float data, *J. Phys. Oceanogr.*, *19*(9), 1177–1190.

Bower, A. S. (1991), A simple kinematic mechanism for mixing fluid parcels across a meandering jet, *J. Phys. Oceanogr.*, *21*(1), 173–180.

Bower, A. S., and M. S. Lozier (1994), A closer look at particle exchange in the Gulf Stream, *J. Phys. Oceanogr.*, *24*(6), 1399–1418.

Bower, A. S., H. T. Rossby, and J. L. Lillibridge (1985), The Gulf Stream—Barrier or blender?, *J. Phys. Oceanogr.*, *15*(1), 24–32.

Churchill, J. H., P. C. Cornillon, and P. Hamilton (1989), Velocity and hydrographic structure of subsurface shelf water at the Gulf Stream's edge, *J. Geophys. Res.*, *94*(C8), 10,791–10,800, doi:10.1029/JC094iC08p10791.

D'Asaro, E., C. Lee, L. Rainville, R. Harcourt, and L. Thomas (2011), Enhanced turbulence and energy dissipation at ocean fronts, *Science*, *332*(6027), 318–322.

D'Asaro, E. A. (2003), Performance of autonomous Lagrangian floats, *J. Atmos. Oceanic Technol.*, *20*(6), 896–911.

Firing, E., J. M. Hummon, and T. K. Chereskin (2012), Improving the quality and accessibility of current profile measurements in the Southern Ocean, *Oceanography*, *25*, 164–165.

Flierl, G., P. Malanotte-Rizzoli, and N. Zabusky (1987), Nonlinear waves and coherent vortex structures in barotropic β-plane jets, *J. Phys. Oceanogr.*, *17*(9), 1408–1438.

Ford, W., J. Longard, and R. Banks (1952), On the nature, occurrence and origin of cold low salinity water along the edge of the Gulf Stream, *J. Mar. Res.*, *11*(3), 281–293.

Gula, J., M. J. Molemaker, and J. C. McWilliams (2014), Submesoscale cold filaments in the Gulf Stream, *J. Phys. Oceanogr.*, *44*(10), 2617–2643.

Gula, J., M. J. Molemaker, and J. C. McWilliams (2015), Gulf Stream dynamics along the southeastern U.S. seaboard, *J. Phys. Oceanogr.*, *45*(3), 690–715.

Johns, W., T. Shay, J. Bane, and D. Watts (1995), Gulf Stream structure, transport, and recirculation near 68°W, *J. Geophys. Res.*, *100*, 817–838.

Joyce, T. M., L. N. Thomas, W. K. Dewar, and J. B. Girton (2013), Eighteen degree water formation within the Gulf Stream during CLIMODE, *Deep Sea Res., Part II*, *91*, 1–10.

Lozier, M., L. Pratt, A. Rogerson, and P. Miller (1997), Exchange geometry revealed by float trajectories in the Gulf Stream, *J. Phys. Oceanogr.*, *27*(11), 2327–2341.

Marshall, J., E. Shuckburgh, H. Jones, and C. Hill (2006), Estimates and implications of surface eddy diffusivity in the Southern Ocean derived from tracer transport, *J. Phys. Oceanogr.*, *36*(9), 1806–1821.

Naveira Garabato, A. C., R. Ferrari, and K. L. Polzin (2011), Eddy stirring in the Southern Ocean, *J. Geophys. Res.*, *116*, C09019, doi:10.1029/2010JC006818.

Pratt, L. J., M. Susan Lozier, and N. Beliakova (1995), Parcel trajectories in quasi geostrophic jets: Neutral modes, *J. Phys. Oceanogr.*, *25*(6), 1451–1466.

Rajamony, J., D. Hebert, and T. Rossby (2001), The cross-stream potential vorticity front and its role in meander-induced exchange in the Gulf Stream, *J. Phys. Oceanogr.*, *31*(12), 3551–3568.

Shchepetkin, A., and J. McWilliams (2005), The regional oceanic modeling system (ROMS): A split-explicit, free-surface, topography-following-coordinate oceanic model, *Ocean Modell.*, *9*(4), 347–404.

Song, T., T. Rossby, and E. Carter (1995), Lagrangian studies of fluid exchange between the Gulf Stream and surrounding waters, *J. Phys. Oceanogr.*, *25*, 46–63.

Stern, M. E. (1985), Lateral wave breaking and "shingle" formation in large-scale shear flow, *J. Phys. Oceanogr.*, *15*(10), 1274–1283.

Thomas, L. N., and T. M. Joyce (2010), Subduction on the northern and southern flanks of the Gulf Stream, *J. Phys. Oceanogr.*, *40*(2), 429–438.

Thomas, L. N., and C. J. Shakespeare (2015), A new mechanism for mode water formation involving cabbeling and frontogenetic strain at thermohaline fronts, *J. Phys. Oceanogr.*, *45*(9), 2444–2456, doi:10.1175/JPO-D-15-0007.1.

Thomas, L. N., J. R. Taylor, E. A. D'Asaro, C. M. Lee, J. M. Klymak, and A. Shcherbina (2016), Symmetric instability, inertial oscillations, and turbulence at the Gulf Stream front, *J. Phys. Oceanogr.*, *46*, 197–217, doi:10.1175/JPO-D-15-0008.1.

Whitt, D. B., and L. N. Thomas (2013), Near-inertial waves in strongly baroclinic currents, *J. Phys. Oceanogr.*, *43*(4), 706–725.